PCCP

PAPER

View Article Online
View Journal | View Issue



Cite this: *Phys. Chem. Chem. Phys.*, 2020, **22**, 24796

# *In situ* anion-doped epitaxial strontium titanate films†

M. Tyunina, *[ab] O. Pacherova,[b] N. Nepomniashchaia, [b] V. Vetokhina,[b] S. Cichon,[b] T. Kocourek[b] and A. Dejneka[b]

Received 8th July 2020,
Accepted 8th October 2020

DOI: 10.1039/d0cp03644g

rsc.li/pccp

Misfit strains arising from a film–substrate mismatch can induce novel phases and properties in the epitaxial films of perovskite oxides. Here we employ yet another effect, namely, strain-assisted formation of oxygen vacancies. We demonstrate the misfit-promoted presence of oxygen vacancies and related substitutional incorporation of anion dopants in the epitaxial films of archetypal perovskite oxide $SrTiO_3$. Both the oxygen vacancies and hydrogen or nitrogen dopants are introduced *in situ* during the pulsed-laser deposition of the films using compressive substrates. The films exhibit peculiar chemical expansion and optical properties, which are consistent with substitutional anion doping.



## Introduction

Strontium titanate ($SrTiO_3$, STO) is an archetypal representative of technologically important perovskite oxide ferroelectrics. Unstressed pure STO crystals are wide-bandgap insulators and adopt a cubic paraelectric state at temperatures above 105 K, and a tetragonal antiferrodistortive phase at lower temperatures. Substitution of Sr can induce ferroelectricity and raise the electrical conductivity in STO.

In addition to cationic doping, substitution of oxygen with anions such as F, H, or N has also been achieved in ferroelectrics. These mixed-anion compounds include high-performance oxyfluoride piezoelectrics, non-toxic oxynitride pigments, and especially valuable oxyhydrides, which can enable solid-state hydride ion conductivity and fast hydrogen exchange and are vital for applications in energy and catalysis (see the review in ref. 1 and references therein).

Because of their metastability, the synthesis of mixed-anion perovskites is a complex process. The most successful method employs the preparation of stoichiometric oxides with the subsequent introduction of anion dopants during high-temperature processing in an anion-containing gas atmosphere. In this work we present the *in situ* synthesis of stable mixed-anion perovskites *via* the epitaxial growth of misfit-strained films.

Cube-on-cube-type epitaxial perovskite oxide films experience misfit strain that arises from a film–substrate mismatch in lattice parameters. This strain is a powerful tool to create new phases and properties in epitaxial films.[2] For instance, the state-of-the-art strain-temperature phase diagram of epitaxial STO films suggests the room-temperature tetragonal antiferrodistortive or ferroelectric phases, which are not available in STO crystals.[3]

Another recently revealed essential consequence of misfit strain is the reduction of the formation energy for oxygen vacancies ($V_O$) in perovskite oxides.[4–7] These oxygen vacancies may offer unoccupied lattice sites for anion dopants, therefore, the misfit-promoted formation of oxygen vacancies may facilitate the substitutional incorporation of anion dopants in epitaxial films. Moreover, as recently found in epitaxial $BaTiO_3$ films,[8,9] a misfit strain can control the orientation of the Ti–$V_O$–Ti complexes and determine the specific locations of the vacancies in selected atomic planes. Hence, misfit-assisted anion doping may lead to specific spatial distribution of dopants as well. Here we experimentally demonstrate such doping in representative STO films.

We employed in-plane compressive misfit strains and varied the gas atmosphere to introduce oxygen vacancies, hydrogen, or nitrogen *in situ*, during the pulsed-laser deposition (PLD) of epitaxial STO films. We observed a strong out-of-plane chemical expansion that indicates the selective location of dopants. We inspected the optical properties of the films and found dopant-specific near-edge absorption, which points to substitutional incorporation of anion dopants. Furthermore, we identified the main interband optical transitions, which suggest minor if any interstitial incorporation of dopants. Finally, we propose that such strain-assisted *in situ* anion doping can be successfully applied to a broad class of perovskite oxides.

[a] *Microelectronics Research Unit, Faculty of Information Technology and Electrical Engineering, University of Oulu, P. O. Box 4500, FI-90014, Finland. E-mail: marina.tjunina@oulu.fi*
[b] *Institute of Physics of the Czech Academy of Sciences, Na Slovance 2, 18221 Prague, Czech Republic*

† Electronic supplementary information (ESI) available. See DOI: 10.1039/d0cp03644g

## Experimental

Epitaxial STO films were grown by pulsed laser deposition on (001) $(LaAlO_3)_{0.3}(SrAl_{0.5}Ta_{0.5}O_3)_{0.7}$ (LSAT) substrates (MTI Corp.). For both reference and comparison, polycrystalline STO films were also simultaneously grown on Si substrates covered with an amorphous native $SiO_2$ layer ($Si/SiO_2$). Compared to epitaxy-enabling LSAT substrates, the $SiO_2$ layer prevents the epitaxial growth of STO. Dense stoichiometric STO ceramics were used as a target. Substrates were kept at a temperature of 973 K during deposition and the temperature was lowered at a rate of 5 K $min^{-1}$ during post-deposition cooling. The gas pressure was varied for different samples (kept constant during deposition and post-deposition cooling): 20 Pa oxygen for regular films (marked here by O), 5 Pa oxygen for introducing oxygen vacancies ($V_O$), and 5 Pa hydrogen or nitrogen for hydrogen or nitrogen doping, respectively (H or N). The thickness of the films was $\sim$80 nm. Additionally, a 200 nm-thick $V_O$-film was prepared for structural investigations.

The room-temperature crystal structure of the films was studied by high-resolution X-ray diffraction on a D8 DISCOVER diffractometer (Bruker corporation) using Cu K$\alpha$ radiation. $\Theta$–$2\Theta$ scans in the range of $2\Theta$ = (10–130) deg and reciprocal space maps (RSM) in the vicinity of the perovskite (002) and (303) diffractions were acquired. The in-plane (parallel to the substrate surface) and out-of-plane (normal to the substrate surface) lattice parameters were estimated from the positions of the diffraction maxima using LSAT as a reference. The thickness of the films was determined using Laue satellites in the $\Theta$–$2\Theta$ scans and by X-ray reflectometry on the diffractometer. The diffraction and reflectometry data were fitted using LEPTOS software.

The chemical composition of the films and the valence state of the constituent elements were inspected by X-ray photoelectron spectroscopy using a NanoESCA photoelectron emission spectroscopy and microscopy instrument (Oxford Instruments Omicron Nanoscience). The sample excitation was performed using monochromatic Al $K\alpha_{1,2}$ (1486.7 eV), He I (21.2 eV), and Hg (5.2 eV) radiation. The measured binding energies were referenced to the Fermi level $E_F$ = 0 eV. The acquired spectra were processed using CasaXPS software.[10] The peaks' backgrounds were convoluted using Shirley functions. The elemental composition was estimated using Scofield's relative sensitivity factors.

The optical properties of the films were examined using variable angle spectroscopic ellipsometry. The measurements were performed on a J. A. Woollam VUV ellipsometer at room temperature, in a dry nitrogen atmosphere, and at photon energies of (0.75–8.8) eV. Ellipsometric spectra were acquired at five angles of incidence (55° to 80° with 5° step) with an energy step of 0.02 eV. The optical constants of the films were extracted from the spectra of ellipsometric angles using a commercial WVASE32 software package. More details on the ellipsometric procedure can be found elsewhere.[10,11]

## Results and discussion

### Uniaxial chemical expansion

XRD analyses showed a cube-on-cube-type epitaxial growth of the STO films on LSAT [Fig. 1(a–i)]. The STO/LSAT films have

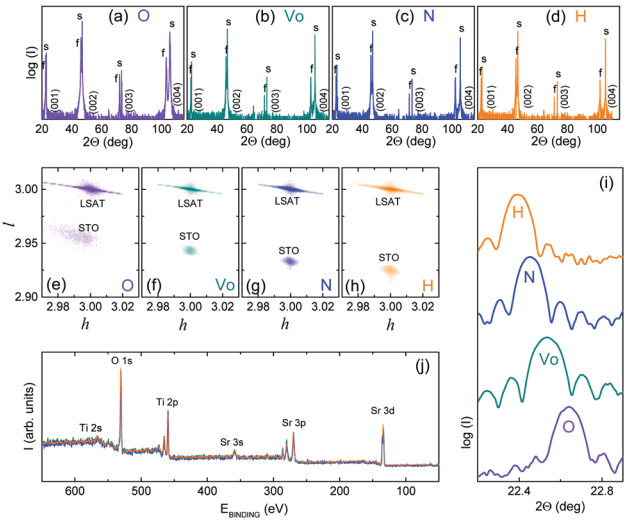


Fig. 1 (a–i) X-ray diffraction (a–d) $\Theta$–$2\Theta$ scans, (e–h) reciprocal space maps along (303) reciprocal lattice points, and (i) comparison of $\Theta$–$2\Theta$ scans around the (001) peak in different films as marked on the plots. Coordinates are expressed in reciprocal lattice units of LSAT in e–h. (j) XPS spectra acquired in the O-, $V_O$, N-, and H-films. The lines of O, Ti, and Sr are marked on the plot.

a perovskite-structure and possess epitaxial relationships [100](001)STO‖[100](001)STO. The $V_O$-, H-, and N-films were perfectly coherent to LSAT [Fig. 1(f–h)], whereas partial relaxation was found in the O-film [Fig. 1(e)].

The lattice parameter of cubic LSAT ($a_{LSAT}$ = 3.868 Å) is smaller than that of cubic STO ($a_{STO}$ = 3.905 Å). Correspondingly, the theoretical biaxial in-plane STO/LSAT misfit strain is compressive: $s_a = (a_{LSAT}/a_{STO} - 1) \approx -0.95\%$. For the coherent strained (001)STO film on (001)LSAT, the in-plane lattice parameters should be similar and equal to $a = a_{LSAT}$ and the out-of-plane lattice parameter $c$ should be elongated, respectively: $c = a_{STO}\cdot[1 - (2c_{12}/c_{11})\cdot s_a] \approx$ 3.927 Å. The elastic constants of STO are $c_{11} = 3.48 \times 10^{11}$ N $m^{-2}$ and $c_{12} = 1.03 \times 10^{11}$ N $m^{-2}$, respectively.[12] As found recently,[3] such tetragonal fully strained STO/LSAT films can grow to a thickness of $<$100 nm, above which the misfit relaxation occurs. In agreement with ref. 3, the 80 nm-thick O-film is tetragonal. The lattice parameters are $c \approx$ 3.926 Å and $a \approx$ 3.870 Å, nearly equal to the theoretically estimated ones.

For oxygen vacancy $V_O$ in STO, the neighboring Ti ions are displaced away from the vacancy and the lattice locally stretches along the Ti–$V_O$–Ti direction.[13–17] This local lattice anisotropy averages out on the macroscopic level for a conventional random spatial distribution of the vacancies; the corresponding chemical lattice expansion is usually isotropic. However, in the epitaxial STO/LSAT films, the in-plane compression can promote the vacancy formation in the Sr–O planes parallel to the substrate (001) surface, *i.e.* in the [Sr–O](001) planes.[7–9] This selective vacancy location is qualitatively comprehensible because the in-plane Ti–$V_O$–Ti elongations "work" against the in-plane misfit compression that is energetically unfavorable. The strain-assisted favorable out-of-plane alignment of the local lattice Ti–$V_O$–Ti elongations can result in a specific preferably out-of-plane macroscopic chemical expansion.

Here, the specific out-of-plane chemical expansion is evidenced by the increased out-of-plane lattice parameter $c_{VO}$ = 3.938 Å in the $V_O$-film compared to the O-film, whereas the in-plane lattice parameters are unchanged therein [Fig. 1(e, f and i)]. Nevertheless, assuming that the large $c_{VO}$ originates from both the isotropic chemical expansion (due to cationic or oxygen off-stoichiometry) of the $V_O$-film material and the film's in-plane compression by LSAT, the lattice parameter of the unstrained cubic $V_O$-material should have been equal to $a_{VO} \approx 3.913$ Å, and the film–substrate misfit strain, correspondingly, $s_{aVO} \approx -1.1\%$. However, the increased magnitude of $s_{aVO}$ suggests a partial strain relaxation and, hence, changes of the in-plane lattice parameters.[3] Instead, the coherency of the $V_O$-film to the LSAT substrate is improved compared to the O-film [Fig. 1(e, f and i)]. The better epitaxial quality of the $V_O$-film is consistent with the out-of-plane alignment of the Ti–$V_O$–Ti complexes that diminishes the total elastic energy.

In order to strongly prove the out-of-plane chemical expansion, we investigated a thicker $V_O$-film (thickness ~200 nm). In the absence of aligned Ti–$V_O$–Ti complexes, the misfit strain was expected to relax.[3] In contrast to this expectation, the film exhibits excellent coherency to LSAT, which evidences the lack of strain relaxation and solidly supports the out-of-plane Ti–$V_O$–Ti orientation [Fig. S1, ESI†].

The out-of-plane chemical expansion is clearly present in the N-films and H-films [Fig. 1(c, d and g–i)], where the out-of-plane elongation is further enhanced: $c_N$ = 3.956 Å and $c_H$ = 3.966 Å. These observations are consistent with the out-of-plane alignment of the Ti–N–Ti and Ti–(H or H2)–Ti complexes and indicate substitutional lattice incorporation of anions.[18–24] We emphasize that interstitial incorporation cannot produce such revealed anisotropic chemical expansion. We note that the deposition conditions do not affect the cationic composition of the films, where the Sr : Ti ratio is close to one [Fig. 1(j) and Fig. S2, ESI†]. In addition, we measured an approximately similar oxygen content in all films within the quantification accuracy of XPS, which suggests oxygen deficiency of $\delta \leq 0.2$ in $SrTiO_{3-\delta}$. However, compared to the O-film, the unit-cell volume is expanded by 0.3% in the $V_O$-film, 0.8% in the N-film, and 1% in the H-film.

We emphasize that the large out-of-plane chemical expansion is achieved in the strained epitaxial STO/LSAT films, whereas the crystal structure and lattice parameters are independent of deposition conditions in polycrystalline films grown on $Si/SiO_2$ [Fig. S3, ESI†]. These observations additionally corroborate the misfit-assisted formation of oxygen vacancies and anion doping. Next, we verify substitutional lattice incorporation of hydrogen or nitrogen by analyzing the optical properties of the films.

### In-gap states

The oxygen vacancies and anion dopants at oxygen sites produce diverse in-gap states in STO.[13–24] Because the optical transitions from/to these states are fingerprints of the vacancies and dopants, investigations of the optical absorption coefficient $\alpha$ can disentangle the vacancy formation and anion interstitial or substitutional incorporation.

The measured optical absorption spectra $\alpha(E)$ reveal the onset of absorption at photon energy $E > 3.5$ eV in all films

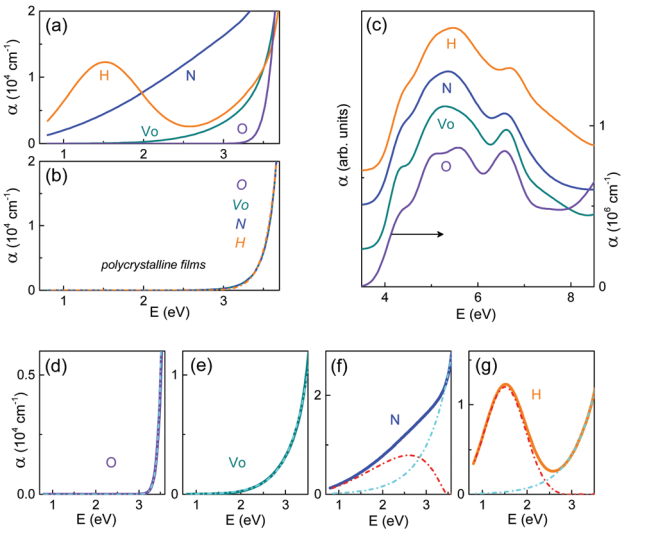


Fig. 2 Optical absorption coefficient $\alpha$ as a function of photon energy in different films as marked on the plots (a–c). The dashed curves show fits to the Urbach rule (d–g) and dopant-specific peaks (f and g, red color).

[Fig. 2(a–c)]. Remarkably, distinct dopant-dependent types of absorption behavior are clearly seen in the near-edge spectral range from 0.7 to ~3.2 eV [Fig. 2(a and b)]. The regular epitaxial O-film [Fig. 2(a)] and all polycrystalline films [Fig. 2(b)] exhibit excellent transparency in this range. This behavior evidences a wide bandgap, in agreement with that in pure STO, and shows the absence of deep in-gap states. The absence of in-gap states is consistent with the absence of a chemical expansion, both of which indicate negligible, if any, concentration of vacancies or dopants.

For optical absorption in STO, a near-edge absorption tail is characteristic and obeys the Urbach rule: $\alpha \propto \exp[(\sigma E)/(k_B T)]$, where the parameter $\sigma$ characterizes the tail steepness, $k_B$ is the Boltzmann constant, and $T$ is the temperature.[25] Good Urbach fits are obtained in the epitaxial O- and $V_O$-films [Fig. 2(d and e)], whereas the Urbach tails are superimposed with dopant-specific absorption peaks in the N- and H-films [Fig. 2(f and g)]. The peaks indicate occupied in-gap states lying ~2.5 eV below the conduction band in the N-film and ~1.5 eV below the conduction band in the H-film.

According to the first-principles analyses,[15,16] the in-gap $V_O$-states are expected to be ~0.2 eV and 0.5 eV below the conduction band and, hence, should not manifest themselves in the spectral range investigated here. The results in Fig. 2(e) are consistent with this expectation.

The deep in-gap states detected here in the N-film [Fig. 2(f)] were not found for the interstitial incorporation of nitrogen in nitrogen-doped (001)STO films.[26] The optically evidenced absence of interstitial nitrogen in our films is confirmed by XPS data: the N 1s lines and shoulders of the Ti 2p lines, which correspond to interstitial nitrogen,[26] are not detected therein. The wide bandgap and the deep in-gap states in the N-film agree well with theoretical calculations,[18,19] which show that the substitution of N for O introduces in-gap states, whereas the mixing of N 2p and O 2p states is very weak and does not reduce

the bandgap. Moreover, our observations of optical absorption at ~2.5 eV are in excellent agreement with the calculations for substitutional N.[20] The results in Fig. 2(f) thus solidly support the substitutional incorporation of nitrogen.

Considering theoretical analyses of hydrogen centers in STO, the observed concurrent strong out-of-plane lattice expansion and optical absorption at ~1.5 eV in the H-film imply the incorporation of one and/or two hydrogen atoms at the oxygen-vacancy site.[21,22] The two atoms can form stable hydrogen molecules ($H_2$) and metastable (2H) complexes. Whereas $H_2$ molecules can produce the strong lattice expansion, they cannot be responsible for the deep in-gap states. The optical absorption at ~1.5 eV is likely caused by the excitation of metastable (2H) complexes.[21] We note that other types of hydrogen-related centers, which are difficult to detect experimentally, may still be present in the H-film. Importantly, our observations reveal a profound substitutional incorporation of hydrogen.

### Interband transitions

For interstitial nitrogen, an uplift of the top valence band and the corresponding narrowing of the optical bandgap are expected.[26] For interstitial hydrogen, the formation energy is low, whereas the related lattice expansion is negligible and not easily seen in chemical expansion. However, a sufficiently large concentration of interstitial hydrogen can lead to an apparent narrowing of the optical bandgap because of the lowering of the conduction band edge.[22] Therefore, a decrease of the energies of the interband optical transitions can signify the presence of interstitial anion dopants in our films.

Here, the near-edge absorption tails prevent from accurate analysis of the indirect bandgap, typical for STO. Good linear fits $(\alpha E)^2 \propto (E - E_d)$ reveal the lowest-energy direct transition being at $E_d \approx 4$ eV in all films [Fig. 3(a–d)]. This energy is ~0.2 eV larger than that (~3.8 eV) in bulk STO.[27] Such a substantial blueshift agrees well with the predicted uplift of the conduction band in epitaxial strained antiferrodistortive STO films.[28] Remarkably, the blueshift increases with increasing out-of-plane elongation in the $V_O$-, N-, and H-films, which also agrees with the predictions.[28] There are no detectable indications of interstitial-induced bandgap narrowing.

The different shapes of the absorption spectra in Fig. 2(c) for different films may be caused by dopant-induced changes in the conduction and/or valence bands. To uncover such changes, we performed closer inspections of the interband transitions *via* critical-point (CP) analysis using the second derivatives of the dielectric functions.[8,29,30] The types of the CP lines are essentially the same in all films [Fig. 3(e–g)]. The energies of the main CPs increase with increasing out-of-plane elongation (from the O-film to the $V_O$-, N-, and H-film, respectively), in qualitative agreement with ref. 27. Additionally, compared to the O-film, the lines are smeared in the spectral range between 5 and 6 eV for all dopant types ($V_O$, N, and H). This observation suggests an effect of oxygen deficiency or substitution rather than interstitial dopants.

Overall, the detected interband transitions are consistent with the effects of lattice strain and oxygen deficiency and/or substitution, while negating appreciable interstitial doping.

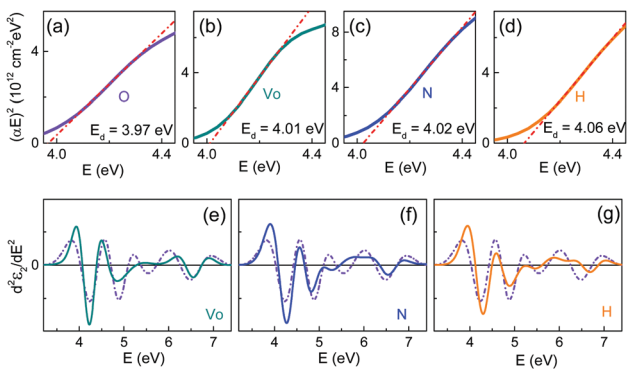


Fig. 3 (a–d) Plots of $(\alpha E)^2$ as a function of photon energy for the direct bandgap in the (a) O-, (b) $V_O$-, (c) N-, and (d) H-films. The dashed lines show fits. (e–g) Second derivative of the imaginary part of the dielectric function $d^2\varepsilon_2/dE^2$ as a function of photon energy in the (e) $V_O$-, (f) N-, and (g) H-films compared to the O-film (dashed curves).

## Conclusions

In conclusion, misfit-assisted *in situ* anion doping is demonstrated in the epitaxial films of archetypal perovskite oxide $SrTiO_3$. Strong out-of-plane chemical expansion is evidenced in the presence of oxygen vacancies and/or nitrogen or hydrogen anion dopants in the cube-on-cube epitaxial films grown on compressive substrates. Substitutional incorporation of anion dopants is indicated by the optical behavior of the films. The observations imply the misfit-promoted formation of oxygen vacancies and oxygen substitution in the Sr–O planes parallel to the substrate surface. This demonstrated approach can be applied to other perovskite oxides such as titanates and rare-earth nickelates.

## Conflicts of interest

There are no conflicts to declare.

## Acknowledgements

The authors acknowledge support from the Czech Science Foundation (Grant No. 19-09671S) and the European Structural and Investment Funds and the Ministry of Education, Youth and Sports of the Czech Republic through Programme "Research, Development and Education" (Project No. SOLID21 – CZ.02.1.01/0.0/0.0/16_019/0000760).

## References

1 H. Kageyama, K. Hayashi, K. Maeda, J. P. Attfield, Z. Hiroi, J. M. Rondinelli and K. R. Poeppelmeier, *Nat. Commun.*, 2018, **9**, 772.
2 N. A. Pertsev, A. G. Zembilgotov and A. K. Tagantsev, *Phys. Rev. Lett.*, 1998, **80**, 1988.

3 T. Yamada, B. Wylie-van Eerd, O. Sakata, A. K. Tagantsev, H. Morioka, Y. Ehara, S. Yasui, H. Funakubo, T. Nagasaki and H. J. Trodahl, *Phys. Rev. B: Condens. Matter Mater. Phys.*, 2015, **91**, 214101.
4 U. Aschauer, R. Pfenninger, S. M. Selbach, T. Grande and N. A. Spaldin, *Phys. Rev. B: Condens. Matter Mater. Phys.*, 2013, **88**, 054111.
5 U. Aschauer and N. A. Spaldin, *Appl. Phys. Lett.*, 2016, **109**, 031901.
6 A. Herklotz, D. Lee, E.-J. Guo, T. L. Meyer, J. R. Petrie and H. N. Lee, *J. Phys.: Condens. Matter*, 2017, **29**, 493001.
7 J. Xi, H. Xu, Y. Zhang and W. J. Weber, *Phys. Chem. Chem. Phys.*, 2017, **19**, 6264.
8 M. Tyunina, D. Chvostova and A. Dejneka, *Phys. Chem. Chem. Phys.*, 2019, **21**, 7874.
9 M. Tyunina, J. Peräntie, T. Kocourek, S. Saukko, H. Jantunen, M. Jelinek and A. Dejneka, *Phys. Rev. Res.*, 2020, **2**, 023056.
10 Casa Software, 2013, www.casaxps.com.
11 A. Dejneka, D. Chvostova, O. Pacherova, T. Kocourek, M. Jelinek and M. Tyunina, *Appl. Phys. Lett.*, 2018, **112**, 031111.
12 *Landolt-Börnstein, Numerical Data and Functional Relationships in Science and Technology, New Series, Group III, Crystal and Solid State Physics*, ed. K. H. Hellwege and A. M. Hellwege, Springer, Berlin, 1981.
13 J. Carrasco, F. Illas, N. Lopez, E. A. Kotomin, Yu. F. Zhukovskii, R. A. Evarestov, Yu. A. Mastrikov, S. Piskunov and J. Maier, *Phys. Rev. B: Condens. Matter Mater. Phys.*, 2006, **73**, 064106.
14 C. Lin, C. Mitra and A. A. Demkov, *Phys. Rev. B: Condens. Matter Mater. Phys.*, 2012, **86**, 161102(R).
15 D. Gryaznov, E. Blokhin, A. Sorokine, E. A. Kotomin, R. A. Evarestov, A. Bussmann-Holder and J. Maier, *J. Phys. Chem. C*, 2013, **117**, 13776.
16 A. Janotti, J. B. Varley, M. Choi and C. G. Van de Walle, *Phys. Rev. B: Condens. Matter Mater. Phys.*, 2014, **90**, 085202.
17 D. Lee, H. Wang, B. A. Noesges, T. J. Asel, J. Pan, J. W. Lee, Q. Yan, L. J. Brillson, X. Wu and C. B. Eom, *Phys. Rev. Mater.*, 2018, **2**, 060403(R).
18 H. F. Liu, *Solid State Commun.*, 2012, **152**, 2063.
19 C. Zhang, Y. Jia, Y. Jing, Y. Yao, J. Ma and J. Sun, *Comput. Mater. Sci.*, 2013, **79**, 69.
20 P. Reunchan, N. Umezawa, A. Janotti, J. T-Thienprasert and S. Limpijumnong, *Phys. Rev. B*, 2017, **95**, 205204.
21 Y. Iwazaki, Y. Gohda and S. Tsuneyuki, *APL Mater.*, 2014, **2**, 012103.
22 J. B. Varley, A. Janotti and C. G. Van de Walle, *Phys. Rev. B: Condens. Matter Mater. Phys.*, 2014, **89**, 075202.
23 T. U. Ito, A. Koda, K. Shimomura, W. Higemoto, T. Matsuzaki, Y. Kobayashi and H. Kageyama, *Phys. Rev. B*, 2017, **95**, 020301(R).
24 T. Misaki, I. Oikawa and H. Takamura, *Chem. Mater.*, 2019, **31**, 7178.
25 N. V. Kurik, *Phys. Status Solidi A*, 1971, **8**, 9.
26 Y. Y. Mi, Z. Yu, S. J. Wang, X. Y. Gao, A. T. S. Wee, C. K. Ong and C. H. A. Huan, *J. Appl. Phys.*, 2007, **101**, 063708.
27 M. Rossle, C. N. Wang, P. Marsik, M. Yazdi-Rizi, K. W. Kim, A. Dubroka, I. Marozau, C. W. Schneider, J. Humlicek, D. Baeriswyl and C. Bernhard, *Phys. Rev. B: Condens. Matter Mater. Phys.*, 2013, **88**, 104110.
28 R. F. Berger, C. J. Fennie and J. B. Neaton, *Phys. Rev. Lett.*, 2011, **107**, 146804.
29 P. Yu and M. Cardona, *Fundamentals of Semiconductors*, Springer, New York, 1996.
30 S. Zollner, A. A. Demkov, R. Liu, P. L. Fejes and R. B. Gregory, *J. Vac. Sci. Technol., B*, 2000, **18**, 2242.